A fully-automatic fast segmentation of the sub-basal layer nerves in corneal images*

Pedro Guimarães, Jeff Wigdahl, Enea Poletti, and Alfredo Ruggeri

***Abstract*— Corneal nerves changes have been linked to damage caused by surgical interventions or prolonged contact lens wear. Furthermore nerve tortuosity has been shown to correlate with the severity of diabetic neuropathy. For these reasons there has been an increasing interest on the analysis of these structures.**

In this work we propose a novel, robust, and fast fully automatic algorithm capable of tracing the sub-basal plexus nerves from human corneal confocal images. We resort to log-Gabor filters and support vector machines to trace the corneal nerves.

The proposed algorithm traced most of the corneal nerves correctly (sensitivity of 0.88 ± 0.06 and false discovery rate of 0.08 ± 0.06). The displayed performance is comparable to a human grader. We believe that the achieved processing time ($0.661 \pm 0.07\ s$) and tracing quality are major advantages for the daily clinical practice.

I. Introduction

The cornea is the most anterior structure of the vertebrate eye and is approximately $500\ \mu m$ thick in the center increasing towards $700\ \mu m$ in the periphery. It has a major role in visual acuity as it is responsible for about two-thirds of the eye's refractive power [1]. It is composed of five layers: the epithelium, the Bowman's layer, the stroma, Descement's membrane and the endothelium. The cornea is known for being one of the most sensitive tissues in the body and it is densely innervated with sensory and autonomic nerves located at the junction between the basal epithelium and the Bowman's layer [2].

Several pathologies and dystrophies that affect the cornea may lead to visual impairment and even to blindness. Other dystrophies may not cause loss of vision but instead repeated pain episodes.

Recently, there has been a particular increasing interest on the analysis of the corneal nerves. Not only because these structures have been shown to provide information about possible damage from surgical interventions (*e.g.*, LASIK or PRK) or from prolonged wear of contact lens [3], [4], [5], but also because it has been shown that some nerve properties are linked to systemic diseases [4], [5], *e.g.*, nerve tortuosity correlates with diabetic neuropathy severity [6], [7].

Confocal microscopy has offered the possibility of imaging the corneal nerves *in vivo* in a fast and non-invasive way. While of major interest, the quantitative analysis of corneal nerves from these images is impractical in the daily clinical practice due to the high number of images, the time consumed *per* image, and the burden of manual or semi-automatic processes. Thus, there is the need for a fully automatic approach capable of accurately and in due time segment the corneal nerves.

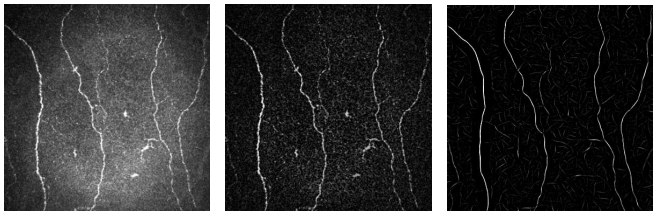

(a) I^{or} (b) I (c) I^{lG}

Fig. 1. From left to right: original (I^{or}), corrected (I), and log-Gabor filtered (I^{lG}) confocal images, respectively.

A few approaches have been proposed over the years to segment the corneal nerves. Scarpa *et al.*[8], applied a fuzzy c-mean clustering technique to classify each pixel as belonging or not to a nerve. In 2011, a new multi-scale dual-model method to detect the corneal nerves was proposed by Dabbah *et al.*[7]. More recently, Poletti and Ruggeri in [9], proposed a method based on a sparse tracking scheme.

In this work we propose a novel, robust, and fast algorithm capable of tracing the sub-basal plexus nerves from human corneal confocal images.

II. Data

A total of 246 confocal microscopy images of the sub-basal corneal nerve plexus of healthy volunteer subjects were acquired using the Heidelberg Retina Tomograph (HRT-II) with the Rostock Cornea Module (Heidelberg Engineering GmbH, Heidelberg, Germany) at the Ophthalmology Department in the Linköping University, Sweden. The imaging instrument was outfitted with a 363/0.95 NA immersion objective lens (Carl Zeiss SMT GmbH, Oberkochen, Germany) to provide confocal images covering a field of $400 \times 400\ \mu m$ (384×384 pixels) (Fig. 1a). The data was split randomly into two different datasets, the training ($N = 50$) and testing ($N = 196$) datasets.

All images were manually segmented by two independent graders (G1 and G2), who traced the centerlines of all visible nerves during several sessions over a 2-weeks period. Both graders used the NeuronJ [10] tracing plugin for ImageJ (publicly available at http://imagej.nih.gov/ij/, 19972014; version 1.45s, Rasband, W.S., ImageJ; National

*This research was made possible by a Marie Curie grant from the European Commission in the framework of the REVAMMAD ITN (Initial Training Research network), Project number 316990.

P. Guimarães, J. Wigdahl, E. Poletti, and A. Ruggeri are with the Department of Information Engineering, University of Padova, Via Gradenigo 6/B, Padova, Italy

978-1-4244-7929-0/14/$26.00 ©2014 IEEE

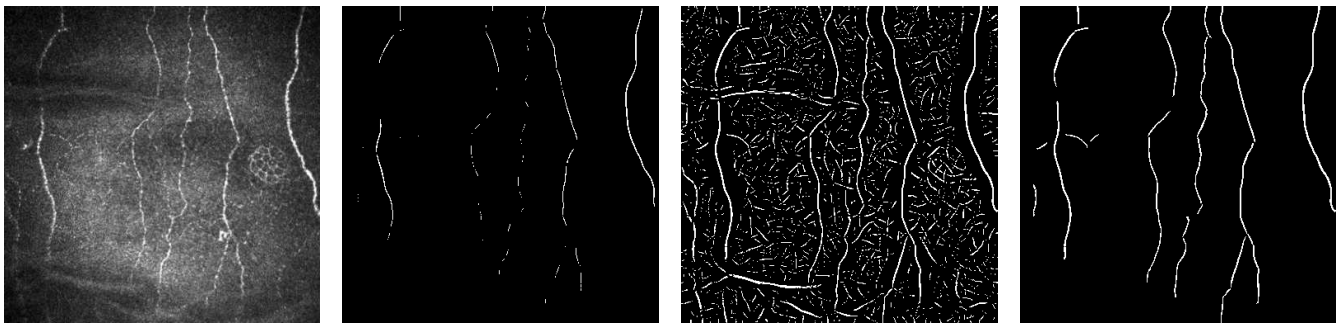

Fig. 2. From left to right: corneal confocal original image and nerves segmentation using an high, low, and hysteresis threshold, respectively.

Institutes of Health, Bethesda, Maryland, USA) over the raw unprocessed images.

The segmentation performed by the G1 grader (S_{G1}) and the intersection between S_{G1} and S_{G2} (S_{Gi}) were used as ground-truth references to evaluate the proposed algorithm.

III. Methods

Throughout this section we describe the proposed nerve segmentation algorithm. We resort to a bank of log-Gabor filters to enhance the corneal nerves. The resulting image is then thresholded to obtain candidate nerve segments that are then classified using a support vector machines (SVM) approach.

A. Image enhancement

Typically, confocal corneal images present uneven illumination and contrast. Particularly noticeable is the difference between the center to the periphery (radially). Although several factors play a role, the spherical-like shape of the cornea has a major influence. As a preprocessing step, all the images undergo top-hat filtering to correct for this issue. This is a widely used method for image enhancement and is computed as the difference between the image and its morphological opening (morphological erosion followed by dilation by a structuring element) [11]. The original and corrected confocal images (respectively I^{or} and I) are shown in Fig. 1a and 1b.

B. Nerve enhancement

Log-Gabor filters are herein applied to enhance the corneal nerves. This filter class has been widely used to detect line-like structures, such as blood vessels, characters for optical character recognition or features for face recognition [12], [13], [14]. Each log-Gabor filter results from the combination of a radial and an angular component, witch limit the filter's frequency (scale) and orientation, respectively. Thus, a log-Gabor filter has a unique orientation-scale combination. The even and odd components of a log-Gabor filter can be obtained as its real and imaginary parts, respectively.

The corrected images are filtered with a bank of log-Gabor even and odd kernels. The used bank covers a wide enough range of scales and orientations to fully describe the corneal nerves. Each value in the final filtered image (I^{lG}) is defined as the difference between the even and odd maximal filter responses, as

$$I^{lG} = \lfloor \max_{no}(I_{no}^{even}) - \max_{no}(\left|I_{no}^{odd}\right|) \rfloor, \tag{1}$$

where I_{no}^{even} and I_{no}^{odd} denote the convolution between image I and the even and odd component (respectively) of a log-Gabor filter of orientation o and scale n. The $\lfloor . \rfloor$ operator assumes the enclosed quantity as zero when negative. Figure 1c shows an example of the filtered image.

C. Nerve segmentation

The usage of a simple threshold to segment line-like structures is in some cases not enough. The resulting nerve segmentation may result in either under-segmentation (unconnected small nerve segments), or over-segmentation (segmentation of noise or other image artefacts). As so, we decided to use hysteresis thresholding instead. This is a popular method for edge detection [15], [16]. It consist in the subsequent usage of two thresholds: one high and one low. Using the high threshold one can be sure that only pixels with high probability of belonging to nerves are selected. Then we apply the low threshold to grow the initial segmentation. Figure 2 shows a corneal confocal image and its segmentation with the high, low, and hysteresis threshold for comparison.

From the thresholding step we obtain candidate nerve segments. These correspond to line-like structures that can be found in the image, but that may or may not be nerves. To distinguish between these two classes, candidate nerve segments are classified resorting to SVM.

SVM is a broadly used supervised-learning method for pattern recognition. This algorithm has been extensively described in the literature [17], [18].

A C-support vector classification with a radial-basis-function kernel was used. The pool of features used in the SVM was computed for each candidate corneal nerve segment and included:

- The mean, standard deviation and range (difference between the largest and smallest values) along the segment path of I^{or}, I, I^{lG} , I_{no}^{even}, and I_{no}^{odd};
- The mean and standard deviation along the segment path of the gradient magnitude and the Laplacian of Gaussian of the image I;

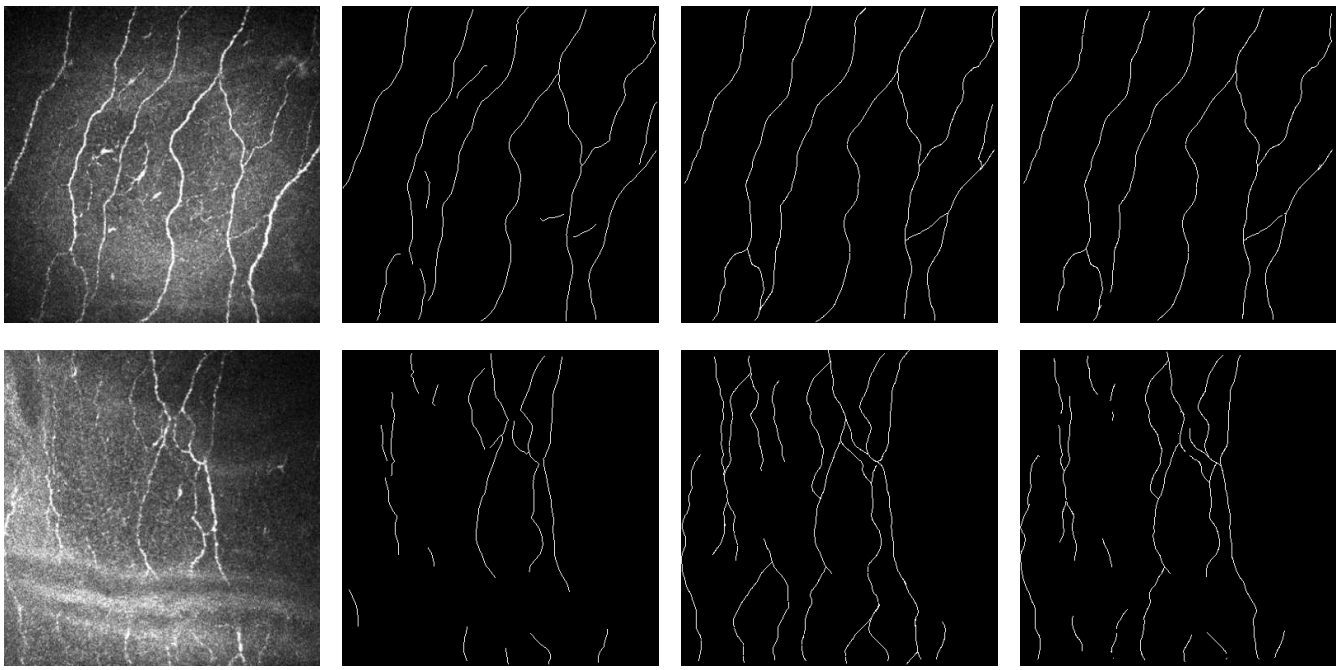

Fig. 3. From left to right: the original images I^{or}, the automatic segmentations S_{A}, and the ground truths S_{G1} and S_{Gi}. The top row shows the case with the highest sensitivity (Sen), while the bottom one the case with the lowest Sen (computed between S_{A} and S_{G1}).

- The length (cumulative distance along the segment's path) and the area (total number of pixels) of the segment.

Feature selection was performed using a backward-elimination approach, based on the accuracy of the segmentation with respect to the ground truth. All algorithm optimization steps, including backward-elimination and parameter optimization, were performed in the training set. The SVM classifier was trained also in this set using the manual segmentation as reference.

IV. Results

To evaluate the algorithm's performance, the nerve tracings obtained by the proposed automatic approach were compared with the reference ground-truths for the testing dataset. Sensitivity (Sen) and false discovery rate (FDR) were computed as

$$Sen \;=\; \frac{\#\left(S_2 \cap m^{dil}(S_1)\right)}{\#\left(S_2\right)} \tag{2}$$

and

$$FDR \;=\; 1 - \frac{\#\left(S_1 \cap m^{dil}(S_2)\right)}{\#\left(S_1\right)}, \tag{3}$$

respectively. The $\#$ operator gives the cardinality, *i.e.*, the number of true pixels (binary 1), and m^{dil} is a morphological dilation operator using a disk with 3 pixels of radius. S_1 and S_2 are two segmentations (binary images) to be compared (S_1 against S_2). Please note that the graders only traced the centerlines of the nerves (see Section II). It is difficult that different specialists chose the same path to trace a given nerve. The morphological dilation (m^{dil} operator) of the binary structures (the corneal nerves segmentations) provides the mandatory tolerance to grader ambiguity.

As stated above, the automatic segmentation achieved by the proposed algorithm (S_{A}) was compared to S_{G1} (chosen over S_{G2} because it presents the highest density of segmented nerves) and the intersection S_{Gi}. The segmentation S_{G2} was also compared to S_{G1} to establish the inter-grader variability. Table I shows the obtained results. Sen gives the proportion of correctly identified nerves, while FDR the proportion of nerves wrongly identified as such.

TABLE I

Sensitivity (Sen) and false discovery rate (FDR) results (average $\pm$ standard deviation, $N = 196$). S_1 and S_2 are the two binary images to be compared. S_{G1}, S_{G2}, S_{Gi}, and S_{A}, are the segmentations obtained by: grader 1, grader 2, the intersection between the two graders, and the proposed automatic approach, respectively.

S_1	S_2	Sen	FDR
S_{G2}	S_{G1}	0.92 ± 0.05	0.08 ± 0.05
S_{A}	S_{G1}	0.86 ± 0.07	0.08 ± 0.07
S_{A}	S_{Gi}	0.88 ± 0.06	0.08 ± 0.06

Overall the proposed algorithm performs well. A higher sensitivity is achieved when S_{A} is compared to the intersection, however the same FDR value is observed. When compared to the inter-grader variability, the algorithm achieves the same FDR. Nevertheless the sensitivity is still slightly lower.

For the visual inspection of the results, Fig. 3 shows the original image I^{or}, the automatic segmentation S_{A}, and the ground truths S_{G1} and S_{Gi} for the best and worst cases (concerning the sensitivity metric).

The time required to analyse a single image, using a single core MATLAB (The MathWorks Inc., Natick, MA) implementation, was 0.61 ± 0.07 s (average $\pm$ standard deviation) on an Intel Core i7-4770 CPU (Intel Corporation, Santa Clara, CA) at 3.4 GHz.

V. Discussion and Conclusions

A fully automatic robust algorithm is of major importance as it can lead to more robust corneal nerve descriptors, such as nerve tortuosity, computed in due time, and consequently the possibility of an improved diagnosis.

The proposed algorithm proved capable to correctly trace most of the corneal nerves. Only a small percentage of the detected nerves are wrongly identified as such. Furthermore the performance level displayed by the proposed approach is comparable to a human grader.

The achieved quality and processing time appear adequate for the possible application of this technique to clinical practice.

Improvements to the algorithm performance are plausible as the achieved segmentations can still benefit from a post-processing stage or a more diverse training set. Time-wise the algorithm performed well. The usage of multicore processing could reduce the time required for the segmentation even further. This might be important especially when considering mosaicing. These issues will be the subject of our research in the future.

Because of its simplicity, the application of the proposed algorithm to different confocal systems should be almost straightforward. However, this will require parameter optimization and SVM training.

The algorithm was not yet tested in pathological cases. Although one might anticipate slightly worst results, please note that the main goal of our research area is to achieve an early diagnosis, and as so, eyes within the early stages of disease progression (close to normal) are the main focus of this technique. Furthermore, we plan to evaluate the proposed approach against already available corneal nerves segmentation algorithms [7], [8], [9].

VI. Acknowledgement

The authors would like to thank Neil Lagali for having kindly provided the confocal images and manual nerve tracings.

References

[1] J. Krachmer, M. Mannis, and E. Holland, *Cornea. Vol. 1*, 2005.

[2] C. F. Marfurt, J. Cox, S. Deek, and L. Dvorscak, "Anatomy of the human corneal innervation," *Experimental eye research*, vol. 90, no. 4, pp. 478–492, 2010.

[3] S. V. Patel, J. W. McLaren, D. O. Hodge, and W. M. Bourne, "Confocal microscopy in vivo in corneas of long-term contact lens wearers," *Investigative ophthalmology & visual science*, vol. 43, no. 4, pp. 995–1003, 2002.

[4] D. V. Patel and C. N. McGhee, "In vivo confocal microscopy of human corneal nerves in health, in ocular and systemic disease, and following corneal surgery: a review," *British Journal of Ophthalmology*, vol. 93, no. 7, pp. 853–860, 2009.

[5] A. Cruzat, D. Pavan-Langston, and P. Hamrah, "In vivo confocal microscopy of corneal nerves: analysis and clinical correlation," in *Seminars in ophthalmology*, vol. 25, no. 5-6. Informa Healthcare New York, 2010, pp. 171–177.

[6] P. Kallinikos, M. Berhanu, C. ODonnell, A. J. Boulton, N. Efron, and R. A. Malik, "Corneal nerve tortuosity in diabetic patients with neuropathy," *Investigative ophthalmology & visual science*, vol. 45, no. 2, pp. 418–422, 2004.

[7] M. Dabbah, J. Graham, I. Petropoulos, M. Tavakoli, and R. Malik, "Automatic analysis of diabetic peripheral neuropathy using multi-scale quantitative morphology of nerve fibres in corneal confocal microscopy imaging," *Medical image analysis*, vol. 15, no. 5, pp. 738–747, 2011.

[8] F. Scarpa, E. Grisan, and A. Ruggeri, "Automatic recognition of corneal nerve structures in images from confocal microscopy," *Investigative ophthalmology & visual science*, vol. 49, no. 11, pp. 4801–4807, 2008.

[9] E. Poletti and A. Ruggeri, "Automatic nerve tracking in confocal images of corneal subbasal epithelium," in *Computer-Based Medical Systems (CBMS), 2013 IEEE 26th International Symposium on*. IEEE, 2013, pp. 119–124.

[10] E. Meijering, M. Jacob, J.-C. Sarria, P. Steiner, H. Hirling, and M. Unser, "Design and validation of a tool for neurite tracing and analysis in fluorescence microscopy images," *Cytometry Part A*, vol. 58, no. 2, pp. 167–176, 2004.

[11] P. Soille, *Morphological image analysis: principles and applications*. Springer-Verlag New York, Inc., 2003.

[12] J. Soares, J. Leandro, R. J. Cesar, H. Jelinek, and M. Cree, "Retinal vessel segmentation using the 2-d gabor wavelet and supervisedclassification," *IEEE Trans Med Imaging*, vol. 25, no. 9, pp. 1214–1222, September 2006.

[13] C. Mancas-Thillou and B. Gosselin, "Character segmentation-by-recognition using log-gabor filters," in *Pattern Recognition, 2006. ICPR 2006. 18th International Conference on*, vol. 2. IEEE, 2006, pp. 901–904.

[14] C. Xu, S. Li, T. Tan, and L. Quan, "Automatic 3d face recognition from depth and intensity gabor features," *Pattern Recognition*, vol. 42, no. 9, pp. 1895–1905, 2009.

[15] C. Harris and M. Stephens, "A combined corner and edge detector." in *Alvey vision conference*, vol. 15. Manchester, UK, 1988, p. 50.

[16] J. Canny, "A computational approach to edge detection," *Pattern Analysis and Machine Intelligence, IEEE Transactions on*, no. 6, pp. 679–698, 1986.

[17] R. O. Duda, P. E. Hart, and D. G. Stork, *Pattern classification*. John Wiley & Sons, 2012.

[18] C.-C. Chang and C.-J. Lin, "LIBSVM: A library for support vector machines," *ACM Transactions on Intelligent Systems and Technology*, vol. 2, pp. 27:1–27:27, 2011, software available at http://www.csie.ntu.edu.tw/~cjlin/libsvm.